Journal of Computational and Applied Mathematics 259 (2014) 730–740

Contents lists available at ScienceDirect

Journal of Computational and Applied Mathematics

journal homepage: www.elsevier.com/locate/cam

DRBEM solution of mixed convection flow of nanofluids in enclosures with moving walls

S. Gümgüm [a,*], M. Tezer-Sezgin [b,1]

[a] Department of Mathematics, İzmir University of Economics, 35330, İzmir, Turkey

[b] Department of Mathematics, Institute of Applied Mathematics, Middle East Technical University, 06531, Ankara, Turkey

ARTICLE INFO

Article history:
Received 23 December 2012
Received in revised form 27 March 2013

Keywords:
Nanofluids
DRBEM
Mixed convection
Lid-driven
Heat source
BEM

ABSTRACT

This paper presents the results of a numerical study on unsteady mixed convection flow of nanofluids in lid-driven enclosures filled with aluminum oxide and copper–water based nanofluids. The governing equations are solved by the Dual Reciprocity Boundary Element Method (DRBEM), and the time derivatives are discretized using the implicit central difference scheme. All the convective terms and the vorticity boundary conditions are evaluated in terms of the DRBEM coordinate matrix. Linear boundary elements and quadratic radial basis functions are used for the discretization of the boundary and approximation of inhomogeneity, respectively. Solutions are obtained for several values of volume fraction (φ), the Richardson number (Ri), heat source length (B), and the Reynolds number (Re). It is disclosed that the average Nusselt number increases with the increase in volume fraction, and decreases with an increase in both the Richardson number and heat source length.

1. Introduction

Nanofluids are the mixture of nano-sized particles suspended in a base fluid. Base fluids, such as water, engine oil and ethylene glycol have low heat transfer performance. Therefore, various techniques are applied to enhance the heat transfer of these fluids. One of them is the use of solid particles as an additive suspended into the base fluid. The improved heat transfer performance of nanofluids is due to the fact that dispersing high thermal conductivity nanoparticles in a base fluid increases the thermal conductivity of such mixtures, and enhances their overall heat transfer capability. Mixed convection is an important heat transfer mechanism and has applications in electronic cooling, drying, heat exchangers and insulation of buildings. It is the combination of forced and natural convection. Thus, the effects of both natural and forced convection influence the governing equations [1].

There are a number of recent studies on the mixed convection flow of nanofluids in cavities. Tiwari and Das [2] analyzed the heat transfer augmentation in a two-sided lid-driven differentially heated square cavity utilizing nanofluids with finite volume approach using the SIMPLER algorithm. They found that both the Richardson number and the direction of the moving walls affect the fluid flow and heat transfer in the cavity. In another study, Talebi et al. [3] investigated the laminar mixed convection flows through a copper–water nanofluid in a square lid-driven cavity. They used the finite volume method for the numerical solution, and found that at the fixed Reynolds number, the solid concentration affects the flow pattern and thermal behavior particularly for a higher Rayleigh number. Mahmoodi [4] analyzed the mixed convection fluid flow and heat transfer in lid-driven enclosures filled with the Al_2O_3–water nanofluid numerically using the finite volume method

* Corresponding author. Tel.: +90 232 4888307; fax: +90 232 2792626.
E-mail addresses: sevin.gumgum@ieu.edu.tr, gumgumsevin@hotmail.com (S. Gümgüm), munt@metu.edu.tr (M. Tezer-Sezgin).
1 Tel.: +90 312 2105376; fax: +90 312 2102972.

0377-0427/$ – see front matter
http://dx.doi.org/10.1016/j.cam.2013.05.006

with SIMPLER algorithm. The results show that at low Richardson numbers, a primary counter-clockwise vortex is formed inside the enclosure. Numerical simulation of mixed convection flows in a square lid-driven cavity partially heated from below using nanofluids is studied by Mansour et al. [5]. The finite difference method (FDM) was employed to solve the dimensionless governing equations of the problem. They observed that increasing solid volume fraction leads to decrease in both the activity of the fluid motion and fluid temperature, however, it leads to increase in the corresponding average Nusselt number. In a recent study, Rahman et al. [6] investigated the behavior of nanofluids in an inclined lid-driven triangular enclosure by using the Galerkin finite element method (FEM). They observed that solid volume fraction strongly influenced the fluid flow and heat transfer in the enclosure at the three convective regimes.

In the literature, mixed convection flow of nanofluids in enclosures are simulated using numerical methods which discretize the whole domain of the problem such as FVM, FDM and FEM. Thus, the resulting system of algebraic equations is very large in size due to the large number of nodal points in the region which has to be taken to achieve a good accuracy. On the other hand, the boundary element method discretizes only the boundary of the region reducing the size of the resulting systems. But, a domain integral results in BEM due to the inhomogeneity when the equation is Poisson's type. This causes loss of boundary only nature of BEM. The DRBEM handles this problem by transforming the domain integral to a boundary integral. The DRBEM has also the flexibility of using fundamental solution of Laplace equation which is the main differential operator in mixed convection flow. In DRBEM all the convective terms and derivative type boundary conditions are approximated using coordinate matrix in terms of radial basis functions. These are the main advantages of DRBEM compared to all other domain discretization numerical methods. The application of DRBEM for solving natural convection flow of nanofluids is given by Gümgüm and Tezer-Sezgin [7] which uses FDM—in time and DRBEM—in space domains. The results are provided for Ra values up to 10^6. DRBEM application is extended to solve also the natural convection flow of micropolar fluids by the same authors [8].

In this paper, DRBEM formulation is given for solving mixed convection flow of nanofluid equations in terms of stream function, vorticity and temperature by using the fundamental solution of Laplace equation, and keeping all the other terms as inhomogeneity [9]. The DRBEM reduces all calculations to the evaluation of the boundary integrals discretizing only the boundary of the region. The unknown vorticity boundary conditions and all the spatial derivatives are easily obtained by using coordinate matrix which contains only radial basis functions. DRBEM application of unsteady mixed convection flow of nanofluids gives rise to systems of initial value problems in time which are approximated by implicit Euler scheme. Considerably small number of boundary elements are used resulting in small sized systems to be solved compared to all the other domain discretization methods. All the original unknowns (stream function, vorticity and temperature) are obtained at all transient levels including steady-state at a cheap expense due to the boundary nature of DRBEM. To the best of author's knowledge this is the first application of DRBEM for solving mixed convection flow of nanofluids.

2. Mathematical formulation

The non-dimensional unsteady momentum and energy equations for nanofluids can be written in terms of stream function (ψ), vorticity (ω) and temperature (T), as [4]

$$\begin{aligned}
&\nabla^2\psi = -\omega \\
&\frac{1}{Re}\frac{\mu_{eff}}{\rho_{nf}\nu_f}\nabla^2\omega = \frac{\partial\omega}{\partial t} + u\frac{\partial\omega}{\partial x} + v\frac{\partial\omega}{\partial y} - Ri\frac{(\rho\beta)_{nf}}{\rho_{nf}\beta_f}\frac{\partial T}{\partial x} \\
&\frac{1}{PrRe}\frac{\alpha_{nf}}{\alpha_f}\nabla^2 T = \frac{\partial T}{\partial t} + u\frac{\partial T}{\partial x} + v\frac{\partial T}{\partial y}
\end{aligned} \tag{1}$$

where $(x, y) \in \Omega \subset R^2$, $t > 0$. Ri, Re and Pr are the Richardson, Reynolds and Prandtl numbers, respectively. $\nu_f = \mu_f/\rho_f$ is the kinematic viscosity of the fluid. μ_f and ρ_f are the dynamic viscosity and the density of the fluid. The velocities are given in terms of stream function as $u = \partial\psi/\partial y$, $v = -\partial\psi/\partial x$ and the vorticity is defined by $\omega = \partial v/\partial x - \partial u/\partial y$.

The density ρ_{nf}, the heat capacitance $(\rho C_p)_{nf}$ and the thermal expansion coefficient $(\rho\beta)_{nf}$ of the nanofluid are defined as $\rho_{nf} = (1-\varphi)\rho_f + \varphi\rho_s$, $(\rho C_p)_{nf} = (1-\varphi)(\rho C_p)_f + \varphi(\rho C_p)_s$, and $(\rho\beta)_{nf} = (1-\varphi)(\rho\beta)_f + \varphi(\rho\beta)_s$, respectively [4,10]. The effective dynamic viscosity of the nanofluid is taken in the first problem as in [4,11], $\mu_{eff} = \mu_f(1+7.3\varphi+123\varphi^2)$, and in the second problem as in [5], $\mu_{eff} = \mu_f/(1-\varphi)^{2.5}$. The effective thermal conductivity of the nanofluid is approximated by the Maxwell–Garnett's model [12], $\kappa_{eff} = \left[\frac{\kappa_s+2\kappa_f-2\varphi(\kappa_f-\kappa_s)}{\kappa_s+2\kappa_f+\varphi(\kappa_f-\kappa_s)}\right]\kappa_f$. The use of this equation is restricted to spherical nanoparticles where it does not account for other shapes of nanoparticles. This model is found to be appropriate for studying heat transfer enhancement using nanofluids [13]. The thermal diffusivity of the nanofluid is given as [4], $\alpha_{nf} = \kappa_{eff}/(\rho C_p)_{nf}$. φ is nanoparticle volume fraction. eff, nf, s and f refer to effective, nanofluid, solid and fluid, respectively. ($\varphi = 0$ refers to pure base fluid and $0 < \varphi \leq 0.2$ refers to nanofluid.)

The equations in (1) are supplied with the appropriate initial and boundary conditions according to the physics of the mixed convective flow of nanofluids in lid-driven enclosures. The fluid in the cavity is a water-based nanofluid containing aluminum oxide (Al_2O_3) and copper (Cu) nanoparticles. It is assumed that the base fluid and nanoparticles are in thermal

equilibrium and no slip occurs between them. The thermo-physical properties of the nanofluid are assumed to be constant except for the density variation, which is approximated by the Boussinesq model.

3. Numerical approach

The DRBEM transforms the differential equations in (1) into boundary integral equations by using the fundamental solution of Laplace equation, $u^* = \frac{1}{2\pi}\ln\left(\frac{1}{r}\right)$. It keeps all the terms other than the diffusion term as inhomogeneity. For this, equations in (1) are weighted through the domain Ω as in [9], by the fundamental solution u^*. Then, Green's second identity is applied and the following integral equations are obtained for each source point i

$$\begin{aligned}
&c_i\psi_i + \int_\Gamma ({\psi_q}^*\psi - \psi^*\psi_q)d\Gamma = \int_\Omega (-\omega)\psi^* d\Omega \\
&\frac{1}{Re}\frac{\mu_{eff}}{\rho_{nf}\nu_f}\left(c_i\omega_i + \int_\Gamma ({\omega_q}^*\omega - \omega^*\omega_q)d\Gamma\right) = \int_\Omega \left(\frac{\partial\omega}{\partial t} + u\frac{\partial\omega}{\partial x} + v\frac{\partial\omega}{\partial y} - Ri\frac{(\rho\beta)_{nf}}{\rho_{nf}\beta_f}\frac{\partial T}{\partial x}\right)\omega^* d\Omega \\
&\frac{1}{PrRe}\frac{\alpha_{nf}}{\alpha_f}\left(c_iT_i + \int_\Gamma ({T_q}^*T - T^*T_q)d\Gamma\right) = \int_\Omega \left(\frac{\partial T}{\partial t} + u\frac{\partial T}{\partial x} + v\frac{\partial T}{\partial y}\right)T^* d\Omega
\end{aligned} \tag{2}$$

where $c_i = \theta_i/2\pi$ with the internal angle θ_i at the source point i. ${\psi}^*$, ${\omega_q}^*$, and ${T}^*$ denote the same fundamental solution u^* of Laplace equation.

In order to transform the domain integrals in Eq. (2) into boundary integrals, we expand the inhomogeneities in each equation by using the radial basis functions f_j's (coordinate radial basis functions), [9]

$$\begin{aligned}
&-\omega \approx \sum_{j=1}^{M+N}\alpha_j f_j(x,y) \\
&\frac{\partial\omega}{\partial t} + u\frac{\partial\omega}{\partial x} + v\frac{\partial\omega}{\partial y} - Ri\frac{(\rho\beta)_{nf}}{\rho_{nf}\beta_f}\frac{\partial T}{\partial x} \approx \sum_{j=1}^{M+N}\bar{\alpha}_j(t)f_j(x,y) \\
&\frac{\partial T}{\partial t} + u\frac{\partial T}{\partial x} + v\frac{\partial T}{\partial y} \approx \sum_{j=1}^{M+N}\tilde{\alpha}_j(t)f_j(x,y).
\end{aligned} \tag{3}$$

In the above equations, $\bar{\alpha}_j$ and $\tilde{\alpha}_j$ are unknown time dependent coefficients whereas α_j are undetermined constants. Here, r is the distance between the source and the field points. Since the radial basis functions are related to the Laplace operator (i.e. $\nabla^2\hat{u} = f$, [9]), one can use the same idea to the right-hand side of the equations in Eq. (2) after substituting the expansions in Eq. (3).

$$\begin{aligned}
&c_i\psi_i + \int_\Gamma ({\psi_q}^*\psi - \psi^*\psi_q)d\Gamma = \sum_{j=1}^{M+N}\alpha_j\left[c_i\hat{u}_{ji} + \int_\Gamma ({\psi_q}^*\hat{u}_j - \psi^*\hat{u}_{q_j})d\Gamma\right] \\
&\frac{1}{Re}\frac{\mu_{eff}}{\rho_{nf}\nu_f}\left(c_i\omega_i + \int_\Gamma ({\omega_q}^*\omega - \omega^*\omega_q)d\Gamma\right) = \sum_{j=1}^{M+N}\bar{\alpha}_{j(t)}\left[c_i\hat{u}_{ji} + \int_\Gamma ({\omega_q}^*\hat{u}_j - \omega^*\hat{u}_{q_j})d\Gamma\right] \\
&\frac{1}{PrRe}\frac{\alpha_{nf}}{\alpha_f}\left(c_iT_i + \int_\Gamma ({T_q}^*T - T^*T_q)d\Gamma\right) = \sum_{j=1}^{M+N}\tilde{\alpha}_j(t)\left[c_i\hat{u}_{ji} + \int_\Gamma ({T_q}^*\hat{u}_j - T^*\hat{u}_{q_j})d\Gamma\right]
\end{aligned} \tag{4}$$

where $\hat{u}_{q_j} = \partial\hat{u}_j/\partial n$, and i varies over M boundary or N selected interior nodes, q denotes the normal derivative.

When linear elements are used for the approximation of ψ, ω, T and their normal derivatives on the boundary, we get the equations in matrix–vector form as

$$\begin{aligned}
&\mathbf{H}\boldsymbol{\psi} - \mathbf{G}\boldsymbol{\psi}_\mathbf{q} = (\mathbf{H}\hat{\mathbf{U}} - \mathbf{G}\hat{\mathbf{Q}})\boldsymbol{\alpha} \\
&\frac{1}{Re}\frac{\mu_{eff}}{\rho_{nf}\nu_f}(\mathbf{H}\boldsymbol{\omega} - \mathbf{G}\boldsymbol{\omega}_\mathbf{q}) = (\mathbf{H}\hat{\mathbf{U}} - \mathbf{G}\hat{\mathbf{Q}})\tilde{\boldsymbol{\alpha}} \\
&\frac{1}{PrRe}\frac{\alpha_{nf}}{\alpha_f}(\mathbf{H}\mathbf{T} - \mathbf{G}\mathbf{T}_\mathbf{q}) = (\mathbf{H}\hat{\mathbf{U}} - \mathbf{G}\hat{\mathbf{Q}})\tilde{\boldsymbol{\alpha}}
\end{aligned} \tag{5}$$

where $\mathbf{H}$ and $\mathbf{G}$ matrices are defined for a source point i and each element j by integrals of the normal derivative and fundamental solution itself, respectively, [9]. The matrices $\hat{\mathbf{U}}$ and $\hat{\mathbf{Q}}$ are constructed by taking the corresponding particular

solutions and normal derivatives of particular solutions, respectively, as columns at the $M+N$ points. The unknowns $\boldsymbol{\psi}$, $\boldsymbol{\omega}$, $\mathbf{T}$ and similarly $\boldsymbol{\psi}_\mathbf{q}$, $\boldsymbol{\omega}_\mathbf{q}$, $\mathbf{T}_\mathbf{q}$ are vectors containing values and normal derivatives at the nodes, respectively.

Evaluation of the right-hand sides of each equation in Eq. (3) at all boundary and selected interior $(M+N)$ points yields

$$\begin{aligned}
&\mathbf{H}\boldsymbol{\psi} - \mathbf{G}\boldsymbol{\psi}_\mathbf{q} = (\mathbf{H}\hat{\mathbf{U}} - \mathbf{G}\hat{\mathbf{Q}})\mathbf{F}^{-1}(-\boldsymbol{\omega})\\
&\frac{1}{Re}\frac{\mu_{eff}}{\rho_{nf}\nu_f}(\mathbf{H}\boldsymbol{\omega} - \mathbf{G}\boldsymbol{\omega}_\mathbf{q}) = (\mathbf{H}\hat{\mathbf{U}} - \mathbf{G}\hat{\mathbf{Q}})\mathbf{F}^{-1}\Big(\frac{\partial\boldsymbol{\omega}}{\partial t} + \mathbf{u}\frac{\partial\boldsymbol{\omega}}{\partial x} + \mathbf{v}\frac{\partial\boldsymbol{\omega}}{\partial y} - Ri\frac{(\rho\beta)_{nf}}{\rho_{nf}\beta_f}\frac{\partial\mathbf{T}}{\partial x}\Big)\\
&\frac{1}{PrRe}\frac{\alpha_{nf}}{\alpha_f}(\mathbf{H}\mathbf{T} - \mathbf{G}\mathbf{T}_\mathbf{q}) = (\mathbf{H}\hat{\mathbf{U}} - \mathbf{G}\hat{\mathbf{Q}})\mathbf{F}^{-1}\Big(\frac{\partial\mathbf{T}}{\partial t} + \mathbf{u}\frac{\partial\mathbf{T}}{\partial x} + \mathbf{v}\frac{\partial\mathbf{T}}{\partial y}\Big)
\end{aligned} \tag{6}$$

where $\mathbf{F}$ is the $(M+N)\times(M+N)$ matrix containing coordinate functions f_j's as columns evaluated at $M+N$ points. Space derivatives in Eq. (6) are approximated with $\mathbf{F}$ as $\frac{\partial\mathbf{R}}{\partial x} = \frac{\partial\mathbf{F}}{\partial x}\mathbf{F}^{-1}\mathbf{R}$, where $\mathbf{R}$ denotes $\boldsymbol{\omega}$, $\boldsymbol{\psi}$ and $\mathbf{T}$.

When the convection terms are substituted back into Eq. (6) and the equations are rearranged, we obtain the following linear system of equation for $\boldsymbol{\psi}$, and systems of ordinary differential equations for $\boldsymbol{\omega}$ and $\mathbf{T}$

$$\begin{aligned}
&\mathbf{H}\boldsymbol{\psi} - \mathbf{G}\boldsymbol{\psi}_\mathbf{q} + \tilde{\mathbf{b}} = \mathbf{0}\\
&\mathbf{A}\dot{\boldsymbol{\omega}} - \tilde{\mathbf{H}}\boldsymbol{\omega} + \tilde{\mathbf{G}}\boldsymbol{\omega}_\mathbf{q} - \tilde{\mathbf{c}} = \mathbf{0}\\
&\mathbf{A}\dot{\mathbf{T}} - \tilde{\mathbf{H}}_t\mathbf{T} + \tilde{\mathbf{G}}_\mathbf{t}\mathbf{T}_\mathbf{q} = \mathbf{0}
\end{aligned} \tag{7}$$

where $\tilde{\mathbf{b}}$ and $\tilde{\mathbf{c}}$ are the vectors and $\tilde{\mathbf{G}}$, $\tilde{\mathbf{G}}_\mathbf{t}$, $\tilde{\mathbf{H}}$ and $\tilde{\mathbf{H}}_\mathbf{t}$ are the matrices given as

$$\begin{aligned}
&\tilde{\mathbf{b}} = \mathbf{A}\boldsymbol{\omega}, \qquad \mathbf{A} = (\mathbf{H}\hat{\mathbf{U}} - \mathbf{G}\hat{\mathbf{Q}})\mathbf{F}^{-1}, \qquad \tilde{\mathbf{c}} = Ri\frac{(\rho\beta)_{nf}}{\rho_{nf}\beta_f}\mathbf{A}\frac{\partial\mathbf{T}}{\partial x}\\
&\tilde{\mathbf{G}} = \frac{1}{Re}\frac{\mu_{eff}}{\rho_{nf}\nu_f}\mathbf{G}, \qquad \tilde{\mathbf{G}}_\mathbf{t} = \frac{1}{PrRe}\frac{\alpha_{nf}}{\alpha_f}\mathbf{G}, \qquad \tilde{\mathbf{H}} = \frac{1}{Re}\frac{\mu_{eff}}{\rho_{nf}\nu_f}\mathbf{H} - \mathbf{R}\\
&\tilde{\mathbf{H}}_t = \frac{1}{PrRe}\frac{\alpha_{nf}}{\alpha_f}\mathbf{H} - \mathbf{R}, \qquad \mathbf{R} = \mathbf{A}\Big(\mathbf{u}\frac{\partial\mathbf{F}}{\partial x}\mathbf{F}^{-1} + \mathbf{v}\frac{\partial\mathbf{F}}{\partial y}\mathbf{F}^{-1}\Big).
\end{aligned}$$

In this study, unsteady equations for mixed convection flow of nanofluids are considered for obtaining transient level as well as steady-state solution. The equations are solved iteratively by advancing in the time direction. Finite difference schemes are widely used in discretization of the time derivatives in partial differential equations that occur after the application of the DRBEM to engineering problems [14].

Approximating the derivatives in Eq. (7) with central difference scheme yields

$$\begin{aligned}
&\Big(\frac{\mathbf{A}}{2\Delta t} - \tilde{\mathbf{H}}\Big)\boldsymbol{\omega}^{m+1} + \tilde{\mathbf{G}}\boldsymbol{\omega}_\mathbf{q}^{m+1} = \Big(\frac{\mathbf{A}}{2\Delta t}\Big)\boldsymbol{\omega}^{m-1} + \tilde{\mathbf{c}}^{m+1}\\
&\Big(\frac{\mathbf{A}}{2\Delta t} - \tilde{\mathbf{H}}_t\Big)\mathbf{T}^{m+1} + \tilde{\mathbf{G}}_\mathbf{t}\mathbf{T}_\mathbf{q}^{m+1} = \Big(\frac{\mathbf{A}}{2\Delta t}\Big)\mathbf{T}^{m-1}.
\end{aligned} \tag{8}$$

In the above iterative process the matrices $\tilde{\mathbf{H}}$, $\tilde{\mathbf{H}}_\mathbf{t}$, and the velocity components are calculated using the stream function equation with the vorticity from the m-th level. Hence, the unknown values are obtained from both previous time levels. These systems together with stream function equation in (7) are solved using direct methods after the insertion of boundary and initial conditions.

4. Numerical results and discussion

Two test problems are presented for the solution of unsteady mixed convection flow of nanofluids. The numerical results are reported for several values of the Richardson number (Ri), nanoparticle volume fraction (φ), heat source length (B), and the Reynolds number (Re) for Al_2O_3–water and Cu–water based nanofluids. The Prandtl number is 6.8 which suitable for the physical situation of the problem. The thermo-physical properties of the nanofluids are given in [2,4,5]. For the base fluid; $C_p[\mathrm{J\,kg^{-1}\,K^{-1}}] = 4179$, $\rho[\mathrm{kg\,m^{-3}}] = 997.1$, $\kappa[\mathrm{W\,m^{-1}\,K^{-1}}] = 0.613$, and $\beta[\mathrm{K^{-1}}] = 21\times10^{-5}$. For the Al_2O_3 nanoparticles; $C_p = 765$, $\rho = 3970$, $\kappa = 25$, and $\beta = 0.85\times10^{-5}$. For the Cu nanoparticles; $C_p = 385$, $\rho = 8933$, $\kappa = 401$, and $\beta = 1.67\times10^{-5}$. The other parameters in Eq. (1) are calculated by using these parameter values through relations given in the second paragraph of Section 2.

The discretization is performed by using linear boundary elements. The radial basis function f is taken as $1 + r + r^2$. The computations are carried out until steady-state is reached for all the unknowns ψ, ω and T. The convergence criteria used

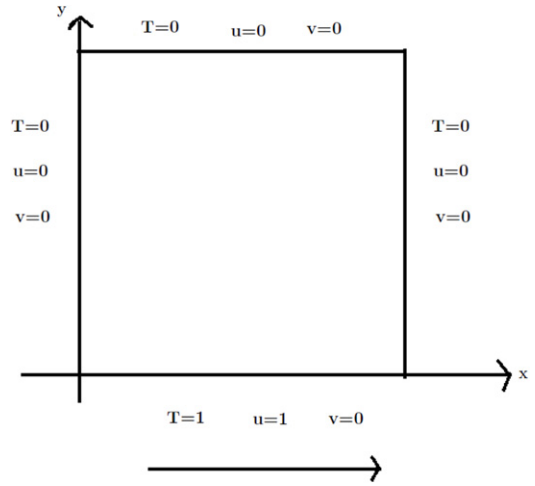

Fig. 1. Layout of Problem 1.

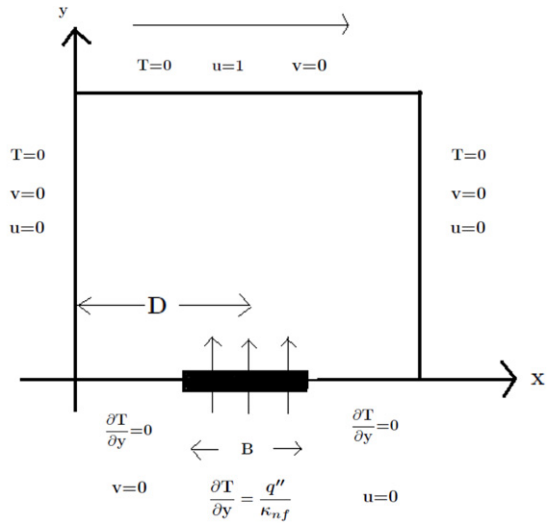

Fig. 2. Layout of Problem 2.

in the time loop to achieve steady-state for vorticity is $\max_{m=1,M+N} |\omega^{(m+1)} - \omega^{(m)}| \leq 10^{-5}$. The same condition is also used for the temperature.

4.1. Problem 1: Square cavity with moving bottom wall

In this problem we consider a square cavity filled with Al_2O_3–water based nanofluid. Corresponding boundary conditions are shown in Fig. 1. The velocity components are zero on the vertical walls and the horizontal top wall resulting with zero stream function value. The horizontal bottom wall is moving with the constant velocity $u = 1$ giving $\partial\psi/\partial y = 1$. The wall at $y = 0$ is heated and the other walls are cooled. Transient behavior is also shown for one particular case of the physical parameters $Ri = 1$ and $\varphi = 0.06$ in Fig. 3. Gr is taken as 10^4 which contains $Re = \sqrt{Gr/Ri}$.

The local and average Nusselt numbers for the heated horizontal bottom wall are defined as in [4]

$$Nu = -\frac{\kappa_{nf}}{\kappa_f}\frac{\partial T}{\partial y}, \qquad Nu_{av} = \int_0^1 Nu(x)dx. \tag{9}$$

Solutions are obtained by using 112, 100 and 96 linear boundary elements for $Ri = 0.1, 1$ and 10 with the time increments $\Delta t = 0.8, 0.3, 0.05$, respectively which are quite large due to the implicit nature of time integration scheme.

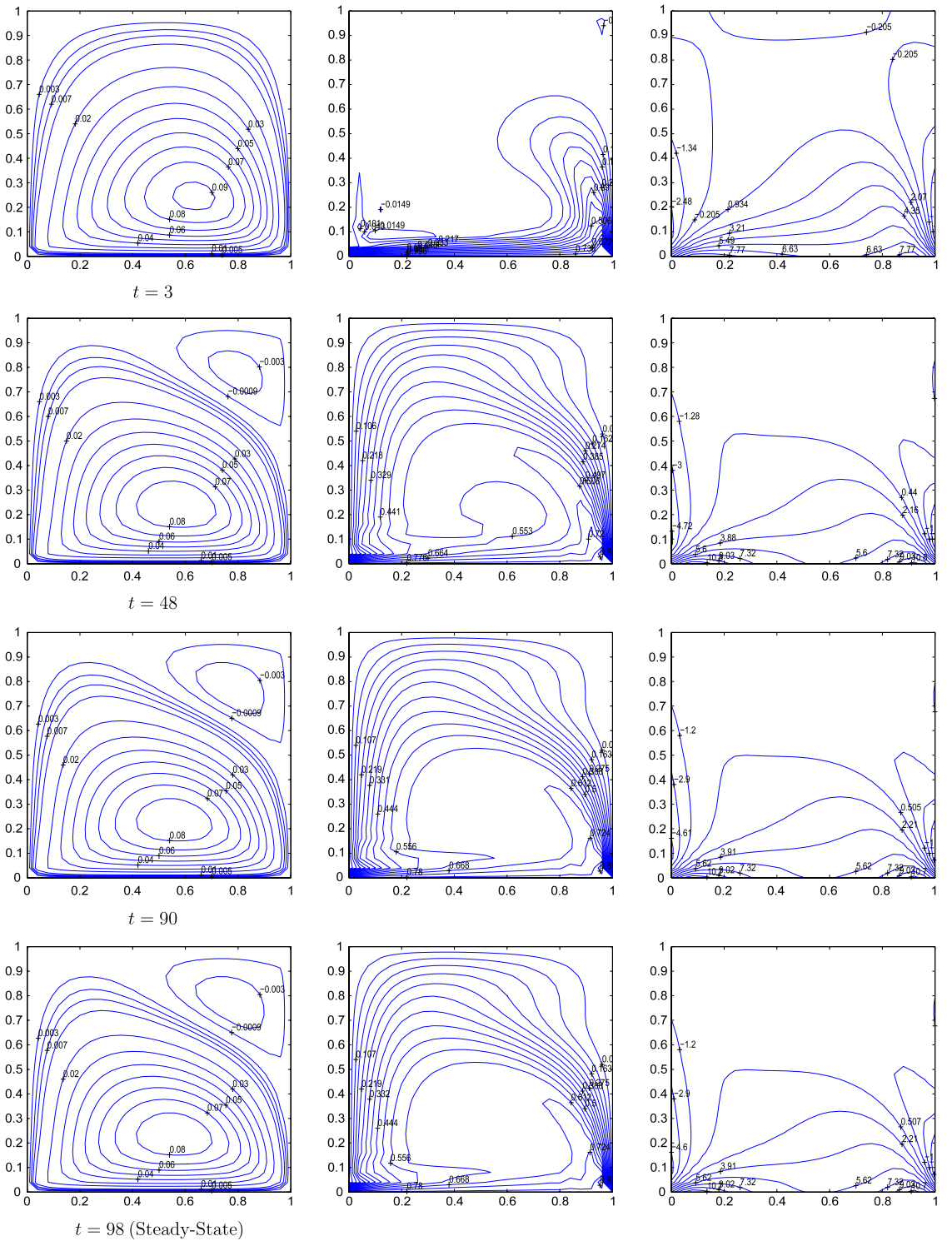

Fig. 3. Transient level behavior of streamlines, isotherms and vorticity for $Ri = 1$ and $\varphi = 0.06$.

In Figs. 4 and 5 we present streamlines and isotherms, respectively for $Ri = 0.1$, 1 and 10 and increasing values of volume fraction $\varphi = 0.0$, 0.03, 0.06 and 0.1. The primary vortex in streamlines decreases in magnitude and tends to move close to the left and bottom walls as Ri increases, meanwhile a secondary vortex enlarges both in magnitude and size in the upper right corner. This behavior is due to the dominance of natural convection compared to the forced convection generated

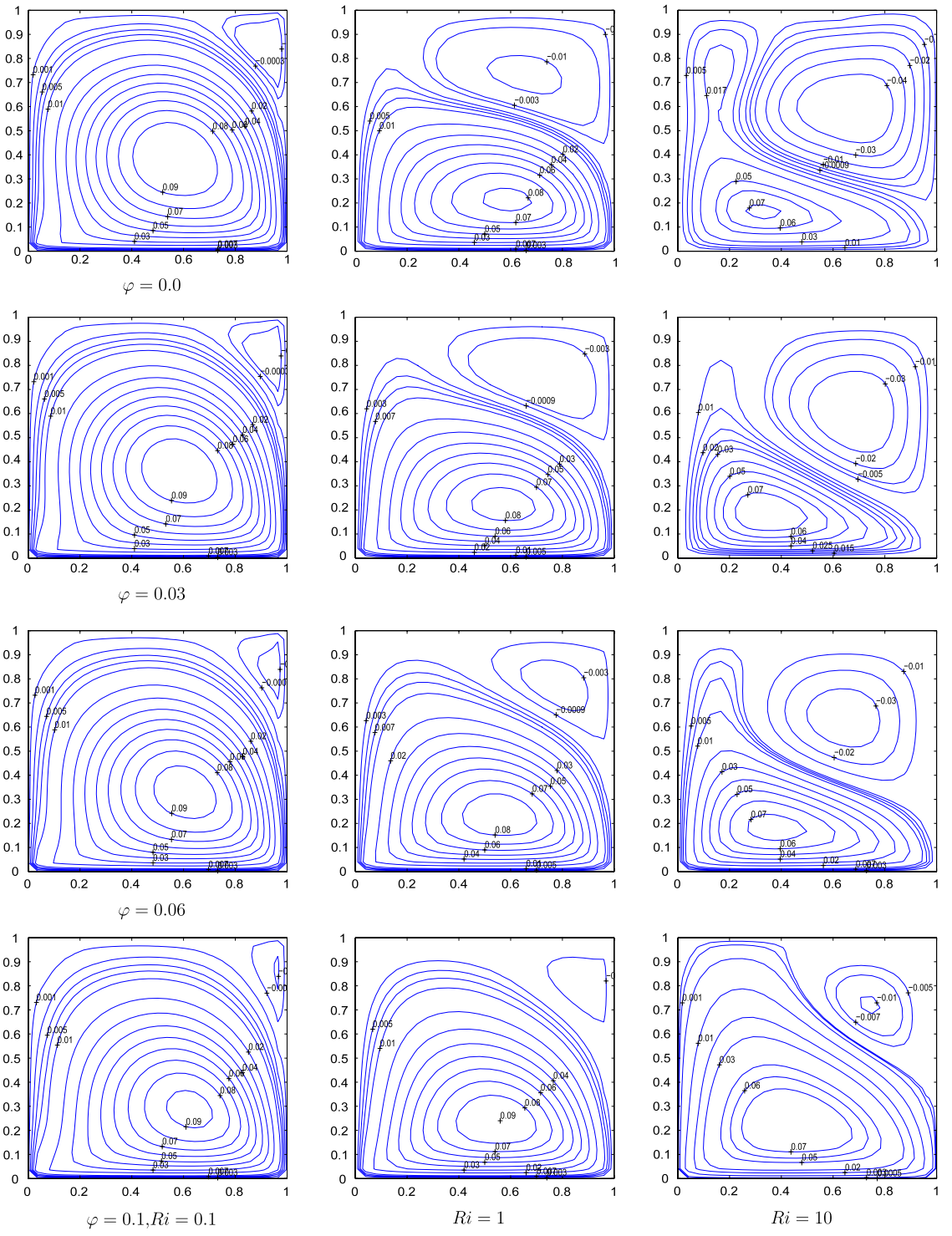

Fig. 4. Streamline contours for $Ri = 0.1$, $Ri = 1$, $Ri = 10$ and several values of volume fraction φ.

by the movement of the bottom wall. As the volume fraction increases secondary vortex lessens in size and strength for a fixed Richardson number. This effect is due to suppression of the natural convection inside the cavity with an increase in the volume fraction of the nanoparticles and resulting an increase in the effective viscosity of the fluid [4]. These behaviors are in good agreement with the results presented by Mahmoodi [4]. Isotherms form boundary layers close to the walls of the cavity when $Ri = 0.1$ for a fixed volume fraction. The center of the cavity is almost stagnant in terms of isotherms.

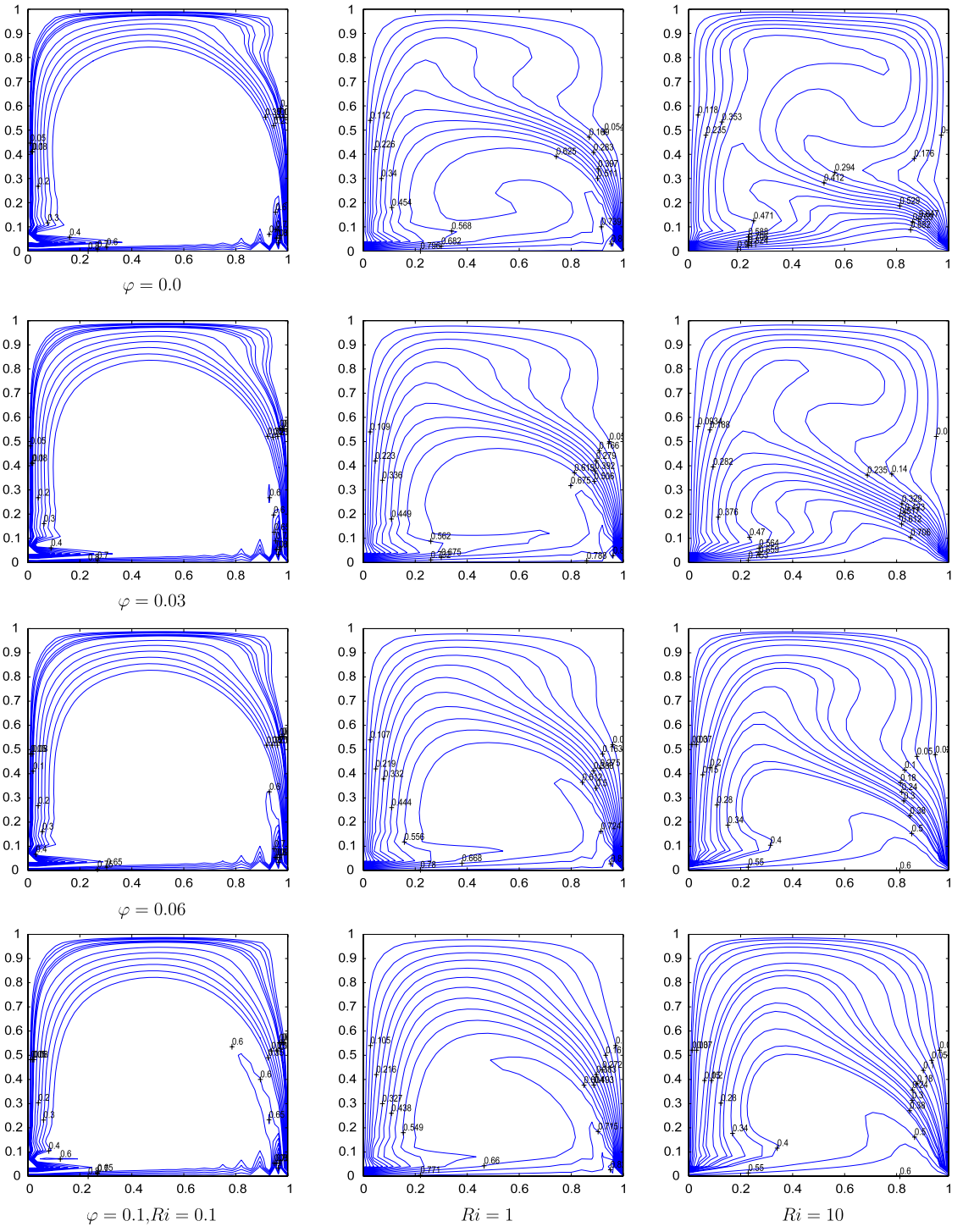

Fig. 5. Isotherm contours for $Ri = 0.1$, $Ri = 1$, $Ri = 10$ and several values of volume fraction φ.

As the Richardson number increases isotherms are evenly distributed inside the cavity due to the dominant effect of natural convection. An increase in volume fraction does not affect the isotherms much when Ri is small. Around $Ri = 1$ (when forced and natural convection are comparable) the core region tends to move close to the bottom heated wall. These behaviors are also observed in [4].

Fig. 6 shows the average Nusselt number values for the considered values of volume fraction and the Richardson number. It can be seen that as the volume fraction increases, the average Nusselt number increases. On the other hand, increasing the

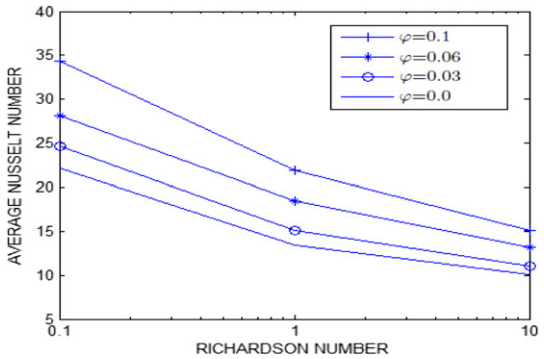

Fig. 6. Average Nusselt number values for $Ri = 0.1$, 1 and 10 with several values of volume fraction.

Table 1
Variation of the average Nusselt number with respect to volume fraction (φ) and heater length (B).

B	$(\varphi) = 0.0$	$(\varphi) = 0.1$	$(\varphi) = 0.2$
0.2	29.37	31.23	32.43
0.8	14.65	15.92	16.92

Richardson number decreases the average Nusselt number, which was also observed in [4]. It is obvious that, the presence of nanoparticles with increasing volume fraction values increases the heat transfer rate significantly.

4.2. Problem 2: Lid-driven cavity with a discrete heater

In the second problem, the cavity is filled with Cu–water based nanofluid and in addition a heater is placed at the bottom wall, [5]. Fig. 2 shows the corresponding boundary conditions. The velocity components are zero on the vertical walls and the horizontal bottom wall. The horizontal top wall is moving with the constant velocity $u = 1$. One part of the bottom wall is heated with a discrete heater while the rest is isolated. The other walls are cooled.

The local and average Nusselt numbers along the heat source surface are defined as in [5]

$$Nu(x) = \frac{1}{T(x)}, \qquad Nu_{av} = \frac{1}{B}\int_{D-0.5B}^{D+0.5B} Nu(x)dx. \tag{10}$$

Computations are carried out for a range of Reynolds number $10 \leq Re \leq 100$, solid volume fraction $0 \leq \phi \leq 0.2$, heat source length $0.2 \leq B \leq 0.8$ and position $0.2 \leq D \leq 0.8$. 88 linear boundary elements are used for $Re = 10$, $B = 0.2$ and $D = 0.2$, and 104 linear boundary elements are used for $Re = 100$, $B = 0.8$ and $D = 0.8$ with a time step $\Delta t = 0.8$.

Fig. 7 $(a_1 - a_2)$ show the effect of the Reynolds number on the streamlines and isotherms for $Ra = 10^3$, $\varphi = 0.1$, $B = 0.4$ and $D = 0.5$. It is observed that for $Re = 10$, the lid-driven effect is not significant and the intensity of the flow are concentrated beside the heat source position. Lid-driven effect becomes significant when the Reynolds number increases. For $Re = 100$, the fluid motion takes place at the top of the cavity and isotherms get close to the left wall of the cavity due to the motion of the upper lid. In Fig. 7 $(b_1 - b_2)$, streamlines and isotherms are simulated for different values of heat source length with $Ra = 10^4$, $Re = 10$, $\varphi = 0.1$ and $D = 0.5$. One can see that the activity of the fluid motion (in terms of magnitude of stream function) and temperature increase with the increase in heat source length. These behaviors are in good agreement with the ones in [5].

Table 1 presents the average Nusselt number values for the considered values of volume fraction and heat source length. It is observed that as the volume fraction increases, the average Nusselt number increases, whereas increasing heat source length decreases the average Nusselt number. The results are in good agreement with the ones given in [5]. The advantage of dispersing nano-sized particles in a base fluid becomes evident in terms of increasing heat transfer rate.

5. Conclusion

The unsteady mixed convection flow of Al_2O_3–water and Cu–water based nanofluids in lid-driven enclosures is studied numerically using the DRBEM. Time derivatives in the equations are discretized by the central difference scheme which is used implicitly. Results are reported for several values of the Richardson number (Ri), nanoparticle volume fraction (φ), heat source length (B), and the Reynolds number (Re) on the momentum and heat transfer. It is observed that the average Nusselt number decreases with an increase in the Richardson number and the heat source length, and increases with the increase in the volume fraction. It is also disclosed that the magnitude of the velocity components increase with an increase in the

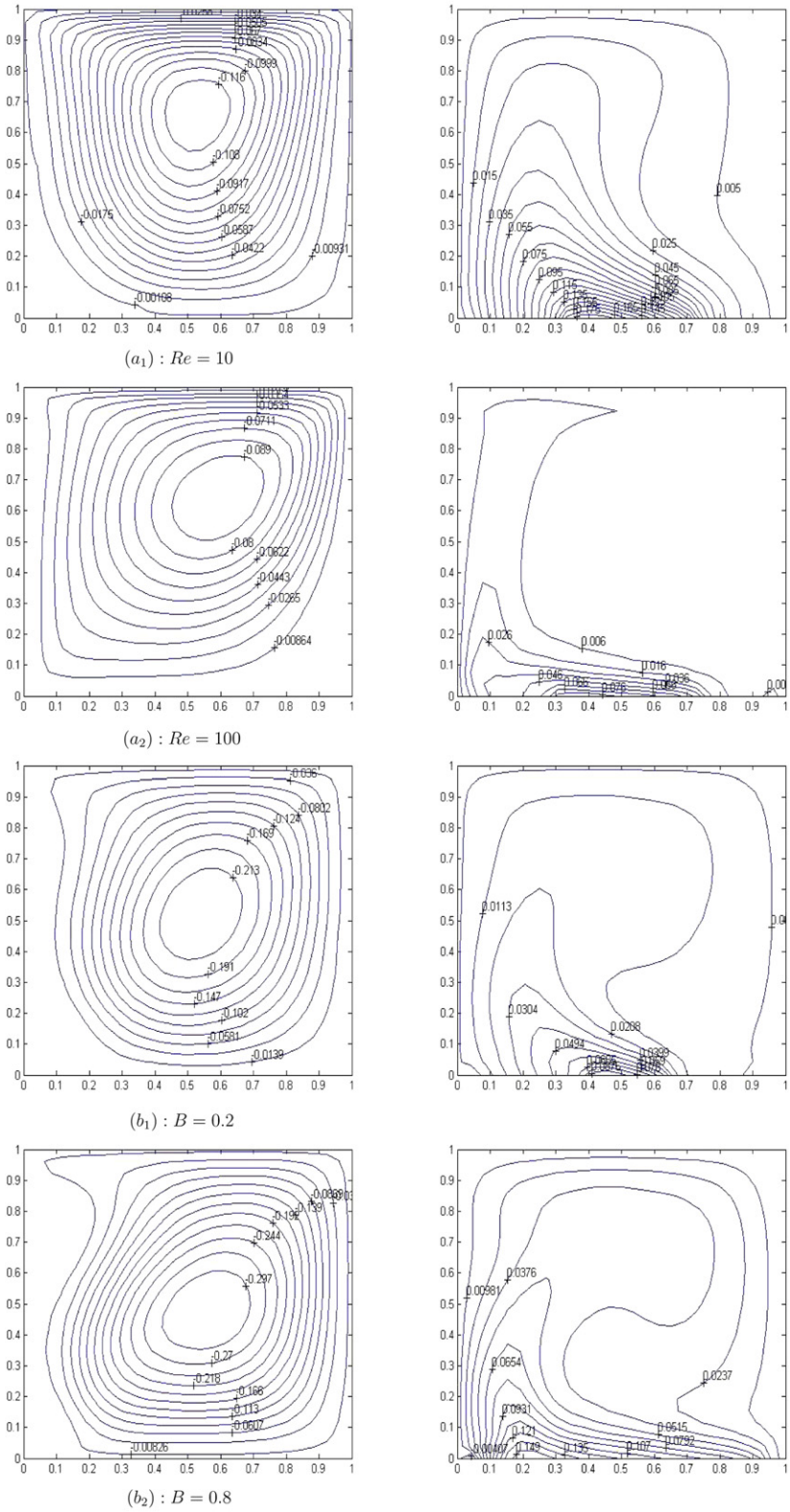

Fig. 7. Streamlines (left) and isotherms (right) for Problem 2. $(a_1 - a_2)$: $Re = 10$ and $Re = 100$, respectively at $Ra = 10^3$, $\varphi = 0.1$, $B = 0.4$, $D = 0.5$. $(b_1 - b_2)$: $B = 0.2$ and $B = 0.8$, respectively at $Ra = 10^4$, $Re = 10$, $\varphi = 0.1$, $D = 0.5$.

volume fraction when *Ri* is kept fixed. Since central difference scheme is used implicitly, time increment does not need to be small. Vorticity boundary conditions and convective terms are evaluated by using the DRBEM coordinate matrix which is an advantage of the method. The DRBEM gives very accurate results with considerably small number of discretized points only on the boundary.

References

[1] F.P. Incropera, D.P. De Witt, Fundamentals of Heat and Mass Transfer, sixth ed., Wiley, 2007.
[2] R.K. Tiwari, M.K. Das, Heat transfer augmentation in a two-sided lid-driven differentially heated square cavity utilizing nanofluids, Int. J. Heat Mass Transfer 50 (2007) 2002–2018.
[3] F. Talebi, A.H. Mahmoodi, M. Shahi, Numerical study of mixed convection flows in a square lid-driven cavity utilizing nanofluid, Int. Commun. Heat Mass Transfer 37 (1) (2010) 79–90.
[4] M. Mahmoodi, Mixed convection inside nanofluid filled rectangular enclosures with moving bottom wall, Therm. Sci. 15 (3) (2011) 889–903.
[5] M.A. Mansour, R.A. Mohamed, M.M. Abd-Elaziz, S.E. Ahmed, Numerical simulation of mixed convection flows in a square lid-driven cavity partially heated from below using nanofluid, Int. Commun. Heat Mass Transfer 37 (2010) 1504–1512.
[6] M.M. Rahman, M.M. Billah, A.T.M.M. Rahman, M.A. Kalam, A. Ahsan, Numerical investigation of heat transfer enhancement of nanofluids in an inclined lid-driven triangular enclosure, Int. Commun. Heat Mass Transfer 38 (10) (2011) 1360–1367.
[7] S. Gümgüm, M. Tezer-Sezgin, DRBEM solution of natural convection flow of nanofluids with a heat source, Eng. Anal. Bound. Elem. 34 (2010) 727–737.
[8] S. Gümgüm, M. Tezer-Sezgin, DRBEM solution of natural convective flow of micropolar fluids, Numer. Heat Transfer, A 57 (2010) 777–798.
[9] P.W. Partridge, C.A. Brebbia, L.C. Wrobel, The Dual Reciprocity Boundary Element Method, in: Comp. Mech. Pub., Southampton and Elsevier Sci., London, 1992.
[10] S.M. Aminossadati, B. Ghasemi, Natural convection cooling of a localised heat source at the bottom of a nanofluid-filled enclosure, European J. Mechanics B/Fluids 28 (5) (2009) 630–640.
[11] S.E.B. Maïga, C.T. Nguyen, N. Galanis, G. Roy, Heat transfer behaviours of nanofluids in a uniformly heated tube, Superlattices Microstruct. 35 (3–6) (2004) 543–557.
[12] J.C. Maxwell, Treatise on Electricity and Magnetism, Oxford University Press, London, 1904.
[13] A. Akbarinia, A. Behzadmehr, Numerical study of laminar mixed convection of a nanofluid in horizontally curved tubes, Appl. Therm. Eng. 27 (8–9) (2007) 1327–1337.
[14] L.C. Wrobel, C.A. Brebbia, D. Nardini, The dual reciprocity boundary element method formulation for transient heat conduction, in: Finite Elements in Water Resources VI, in: Comp. Mech. Pub., Southampton and Springer-Verlag, Berlin and New York, 1986.